Cr3+-Doped Fluorides and Oxides: Role of Internal Fields and Limitations of the Tanabe-Sugano Approach

ARTICLE *in* THE JOURNAL OF PHYSICAL CHEMISTRY A · NOVEMBER 2011

Impact Factor: 2.69 · DOI: 10.1021/jp207249w · Source: PubMed

6 AUTHORS, INCLUDING:

Miguel Moreno
Universidad de Cantabria
224 PUBLICATIONS **2,711** CITATIONS

SEE PROFILE

THE JOURNAL OF PHYSICAL CHEMISTRY A

ARTICLE

pubs.acs.org/JPCA

Cr^{3+}-Doped Fluorides and Oxides: Role of Internal Fields and Limitations of the Tanabe−Sugano Approach

A. Trueba,[†] J. M. García-Lastra,[‡] P. Garcia-Fernandez,[†] J. A. Aramburu,[*,†] M. T. Barriuso,[§] and M. Moreno[†]

[†]Departamento de Ciencias de la Tierra y Física de la Materia Condensada, Universidad de Cantabria, Avenida de los Castros s/n, 39005 Santander, Spain

[‡]Center for Atomic-Scale Materials Design, Department of Physics, Technical University of Denmark, DK-2800 Kongens Lyngby, Denmark

[§]Departamento de Física Moderna, Universidad de Cantabria, Avenida de los Castros s/n, 39005 Santander, Spain

ABSTRACT: This work is aimed at clarifying the changes on optical spectra of Cr^{3+} impurities due to either a host lattice variation or a hydrostatic pressure, which can hardly be understood by means of the usual Tanabe−Sugano (TS) approach assuming that the Racah parameter, *B*, grows when covalency decreases. For achieving this goal, the optical properties of Cr^{3+}-doped $LiBaF_3$ and $KMgF_3$ model systems have been explored by means of high level ab initio calculations on CrF_6^{3-} units subject to the electric field, $\mathbf{E}_R(\mathbf{r})$, created by the rest of the lattice ions. These calculations, which reproduce available experimental data, indicate that the energy, $E(^2E)$, of the $^2E(t_{2g}^3) \rightarrow {}^4A_2(t_{2g}^3)$ emission transition is nearly independent of the host lattice. By contrast, the energy difference corresponding to $^4A_2(t_{2g}^3) \rightarrow {}^4T_1(t_{2g}^2e_g^1)$ and $^4A_2(t_{2g}^3) \rightarrow {}^4T_2(t_{2g}^2e_g^1)$ excitations, $\Delta(^4T_1; {}^4T_2)$, is shown to increase on passing from the normal to the inverted perovskite host lattice despite the increase in covalency, a fact which cannot be accounted for through the usual TS model. Similarly, when the $Cr^{3+}-F^-$ distance, **R**, is reduced both $\Delta(^4T_1; {}^4T_2)$ and the covalency are found to increase. By analyzing the limitations of the usual model, we found surprising results that are shown to arise from the deformation of both 3d(Cr) and ligand orbitals in the antibonding e_g orbital, which has a σ character and is more extended than the π t_{2g} orbital. By contrast, because of the higher stiffness of the t_{2g} orbital, the dependence of $E(^2E)$ with **R** basically follows the corresponding variation of covalency in that level. Bearing in mind the similarities of the optical properties displayed by Cr^{3+} impurities in oxides and fluorides, the present results can be useful for understanding experimental data on Cr^{3+}-based gemstones where the local symmetry is lower than cubic.

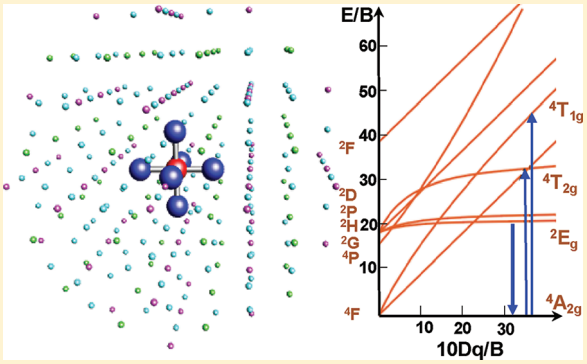

1. INTRODUCTION

For over 50 years, Tanabe−Sugano diagrams have been widely used for characterizing the experimental d−d excitations of transition-metal impurities in insulating lattices.[1−3] Indeed, experimental d−d transitions of impurities like Cr^{3+}, Fe^{3+}, Mn^{2+}, Co^{2+}, or Ni^{2+} in cubic insulating lattices can reasonably be fitted using only three parameters: the cubic field splitting parameter, 10Dq, and two Racah parameters, *B* and *C*, with $C \cong 4.5B$. It is also well-known that the *B* values obtained by this fitting procedure along a series of MX_6 complexes (X = F, Cl, Br, I) for a given 3d cation reveal that *B* decreases following the lowering of ligand electronegativity and thus the increase of covalency in the complex.[4] However, this widely used approach leads to inconsistencies when analyzing small but relevant changes in optical transitions of a transition-metal complex induced either by modifying the host lattice or by a hydrostatic pressure. This work is aimed at clearing out the microscopic origin of such discrepancies.

In order to achieve this goal, the optical properties of model systems $LiBaF_3$:Cr^{3+} and $KMgF_3$:Cr^{3+} have been explored by means of highly correlated multireference ab initio calculations.[5−7] Moreover, additional calculations based on the density functional theory (DFT) have been carried out. In all cases, results have been obtained for different values of the $Cr^{3+}-F^-$ distance, **R**. The host lattices have been chosen because both are cubic but exhibit a different crystal structure. So $LiBaF_3$ has an inverted perovskite structure[8] different from the normal one[9] exhibited by $KMgF_3$ (Figure 1). The results obtained on these model systems can also be of interest in the realm of gemstones like ruby (Al_2O_3:Cr^{3+}), emerald ($Be_3Si_6Al_2O_{18}$:Cr^{3+}), or alexandrite ($BeAl_2O_4$:Cr^{3+}) where the symmetry of the host lattices is lower than cubic.[3,10]

Active electrons of a transition-metal impurity, M, in an insulating lattice are usually confined in the MX_N^{q-} complex formed with the nearest anions, X. Nevertheless, it has been pointed out that optical and magnetic properties associated to

Received: July 29, 2011
Revised: September 28, 2011
Published: October 10, 2011

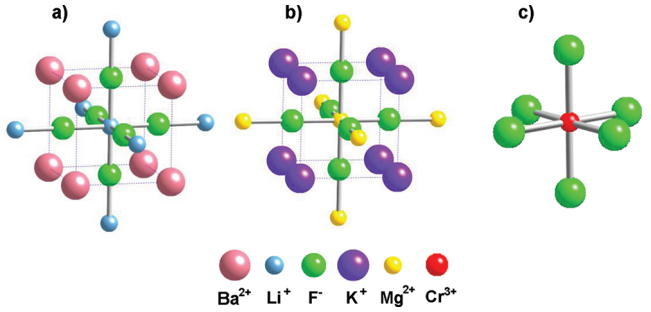

Figure 1. Crystal structures of (a) $KMgF_3$, a normal cubic perovskite, and (b) $BaLiF_3$, an inverted perovskite. (c) The CrF_6^{3-} complex formed by the $Mg^{2+} \rightarrow Cr^{3+}$ or $Li^{+} \rightarrow Cr^{3+}$ substitution in $KMgF_3$ and $BaLiF_3$, respectively.

the impurity cannot be understood considering only the isolated MX_N^{q-} unit at the right equilibrium distance. Indeed, it is necessary to take into account the electric field, $\mathbf{E}_R(\mathbf{r})$, created by the rest of the lattice ions on the active electrons of the complex.[11] This explains that the 10Dq values measured for $LiBaF_3$:M (M = Cr^{3+}, Co^{2+}, Ni^{2+}, Mn^{2}) are found to be systematically about 10−20% higher than that in the case of $KMgF_3$:M despite the fact that the impurity−ligand distance, **R**, is essentially the same for both lattices.[5−7,12−18] Furthermore, the distinct electric field, $\mathbf{E}_R(\mathbf{r})$, in ruby and emerald has been shown to be the main cause behind the different colors of such gemstones mainly determined by the energy, $E(^4T_2)$, of the $^4A_2(t_{2g}^3) \rightarrow {}^4T_2(t_{2g}^2e_g^1)$ transition.[19,11] Indeed, accurate extended X-ray absorption fine structure (EXAFS) measurements carried out in the last years on both $Al_2O_3:Cr^{3+}$ and $Be_3Si_6Al_2O_{18}:Cr^{3+}$ prove that the mean $Cr^{3+}-O^{2-}$ distance is the same within the experimental uncertainty of 1 pm.[20,21]

By looking in more detail into the optical spectra of Cr^{3+} impurities in different oxide or fluoride lattices, we find other subtle differences that are not easy to be understood on a simple basis. Let us call $\Delta(^4T_1; {}^4T_2) = E(^4T_1) - E(^4T_2)$, where $E(^4T_j)$ (j = 1, 2) denotes the energy of the $^4A_2(t_{2g}^3) \rightarrow {}^4T_j(t_{2g}^2e_g^1)$ excitation. The two $E(^4T_j)$ transition energies are well determined in optical absorption as both ^4T_j excited states have the same spin as the ground state $^4A_2(t_{2g}^3)$. The value of $\Delta(^4T_1; {}^4T_2)$ measured for ruby is 6500 cm^{-1}, whereas it is 15% higher for emerald.[10] As in the framework of Tanabe−Sugano diagrams $\Delta(^4T_1; {}^4T_2) \cong 12B$, such a significant difference could in principle be explained through a rather different B Racah parameter for the two gemstones. However, that conclusion is seemingly in contradiction with what is observed for the sharp emission line $^2E(t_{2g}^3) \rightarrow {}^4A_2(t_{2g}^3)$ whose energy, $E(^2E)$, is practically the same for both gemstones despite $E(^2E) = 9B + 3C = 22.5B$ taking $C/B = 4.5$ corresponding to the free Cr^{3+} ion.[1] In fact, the measured $E(^2E)$ values for ruby and emerald, 14 420 and 14 690 cm^{-1}, respectively, differ only by 1.8%.[3,22−25]

Although $E(^2E)$ has not been measured for Cr^{3+}-doped $LiBaF_3$ and $KMgF_3$, the experimental value $\Delta(^4T_1; {}^4T_2)$ = 7190 cm^{-1} measured for the former system[6] is also slightly different from $\Delta(^4T_1; {}^4T_2)$ = 6780 cm^{-1} reported for the latter[5] despite that the calculated $Cr^{3+}-F^{-}$ distance for both systems is the same within 0.7%.[7]

With regard to the variations induced by pressure upon the $^2E(t_{2g}^3) \rightarrow {}^4A_2(t_{2g}^3)$ emission line, a value of $E(^2E)$ = 14 170 cm^{-1} is measured for a hydrostatic pressure equal to 34 GPa for ruby, which implies a decrease of 250 cm^{-1} when compared to a value of $E(^2E)$ = 14 420 cm^{-1} measured at zero pressure.[25] Accordingly, the experimental value $\partial E(^2E)/\partial P = -7$ cm^{-1}/GPa would imply $\partial B/\partial P = -0.3$ cm^{-1}/GPa. However, the reported dependence[25] of $\Delta(^4T_1; {}^4T_2)$ on pressure ($\partial\Delta(^4T_1; {}^4T_2)/\partial P$ = 0.17 ± 0.12 cm^{-1}/GPa) leads to $\partial B/\partial P$ practically equal to zero.

Although in fluorides at zero-pressure the first excited state is $^4T_2(t_{2g}^2e_g^1)$ and not $^2E(t_{2g}^3)$, this situation can be reversed by an applied pressure.[26−28] By virtue of this fact, the pressure dependence of the sharp emission line $^2E(t_{2g}^3) \rightarrow {}^4A_2(t_{2g}^3)$ has recently been measured for $LiCaAlF_6:Cr^{3+}$.[28] Similarly to what happens in the case of ruby or alexandrite, it has been found that $E(^2E)$ decreases when pressure is applied and $\partial E(^2E)/\partial P = -3.5$ cm^{-1}/GPa, a value of the same order as that measured in ruby.[22]

These experimental data thus point out that variations of $\Delta(^4T_1; {}^4T_2)$ and $E(^2E)$ energies corresponding to CrF_6^{3-} or CrO_6^{9-} units induced either by a change of host lattice or by a hydrostatic pressure can hardly be understood within the widely used Tanabe−Sugano framework.

Bearing this analysis in mind, there are two main goals of the present work. On one hand, we want to explore by means of ab initio calculations the changes on optical properties on passing from $KMgF_3:Cr^{3+}$ to $LiBaF_3:Cr^{3+}$ and also the variations of $\Delta(^4T_1; {}^4T_2)$ and $E(^2E)$ due in both cases to a reduction of the $Cr^{3+}-F^{-}$ distance. On the other hand, we pay particular attention to investigate whether these subtle changes can or cannot be accounted for just considering the CrF_6^{3-} unit perturbed by the internal electric field, $\mathbf{E}_R(\mathbf{r})$, of the corresponding host lattices.

The presence of a Cr^{3+} impurity at the Mg^{2+} site in $KMgF_3$ requires the existence of charge compensation. Studies carried out using electron paramagnetic resonance (EPR) and electron nuclear double resonance (ENDOR) techniques prove, however, that in cubic and layered perovskites, like K_2MgF_4, doped with Cr^{3+} or Fe^{3+} impurities, apart from centers involving a close vacancy, cubic CrF_6^{3-} or FeF_6^{3-} centers are also formed where the charge compensation is far apart and thus not detected through any spectroscopic measurement.[5,29−33] Moreover, the optical absorption spectra of centers involving a close vacancy are found to be very close to that for the cubic center.[5] For instance, in $KMgF_3:Cr^{3+}$ there is no observable splitting in the $^4A_2(t_{2g}^3) \rightarrow {}^4T_2(t_{2g}^2e_g^1)$ band for centers containing a close vacancy. Moreover, the optical data reported by Mortier et al. indicate that the $^4A_2(t_{2g}^3) \rightarrow {}^4T_2(t_{2g}^2e_g^1)$ zero-phonon line for the center involving an adjacent Mg^{2+} vacancy is shifted only by ∼100 cm^{-1} with respect to that for the cubic center.[5] Along this line, the center of gravity of the $^4A_2(t_{2g}^3) \rightarrow {}^4T_2(t_{2g}^2e_g^1)$ transition calculated for the center with a Mg^{2+} vacancy is found to be shifted only ∼300 cm^{-1} with respect to 15 150 cm^{-1} measured for the cubic center.[34]

The optical absorption spectra reported for $LiBaF_3:Cr^{3+}$ does not show any departure from cubic symmetry either in the $^4A_2(t_{2g}^3) \rightarrow {}^4T_2(t_{2g}^2e_g^1)$ or in the $^4A_2(t_{2g}^3) \rightarrow {}^4T_1(t_{2g}^2e_g^1)$ bands.[6] Nevertheless, EPR data indicate that most of the formed centers involve a Ba^{2+} vacancy.[6]

This work is arranged as follows: as the present analysis is greatly based on the localization of active electrons the main experimental facts supporting the validity of that approach are briefly recalled in section 2. Relevant details of the employed ab initio methods are given in section 3, whereas the results obtained in this work are discussed in some detail in section 4. Some final remarks are offered in section 5.

2. ELECTRON LOCALIZATION

Electron localization is the fingerprint of an insulating material, a key point stressed by W. Kohn.[35,36] By virtue of this fact, crystal field spectra of pure compounds like $KNiF_3$ or Cr_2O_3 look rather similar to those observed for $KMgF_3:Ni^{2+}$ or $Al_2O_3:Cr^{3+}$.[11,37] Furthermore, if unpaired electrons coming from the transition-metal impurity, M, in $Al_2O_3:Cr^{3+}$ or $KMgF_3:Ni^{2+}$ are essentially localized in the MX_6^{q-} complex (X = O, F) formed with the six X ligands, the understanding of the properties associated with the impurity can be greatly simplified. Indeed, they can reasonably be accounted for merely considering the complex under the influence of the electric field, $\mathbf{E}_R(\mathbf{r})$, created by the rest of lattice ions.[11]

Crucial experimental information on the degree of localization for the impurities in insulating lattices is provided by ENDOR data. For instance, in cases like $KMgF_3:Mn^{2+}$, apart from the average hyperfine constant for ligands, $A_s(1)$, the corresponding constant, $A_s(2)$, for the nearest F^- ions lying outside the MnF_6^{4-} complex, have also been measured.[38] The values $A_s(1) = 54$ MHz and $A_s(2) = 0.64$ MHz thus support that active electrons are essentially localized on the MnF_6^{4-} unit. In the case of systems like $Al_2O_3:Cr^{3+}$, there is no hyperfine interaction with ligands because the nuclear spin of the ^{16}O isotope is zero. However, the hyperfine interaction with the closest aluminum ions has been measured by ENDOR obtaining an isotropic hyperfine constant, $A_s(Al)$, around 2 MHz.[39] Bearing in mind that an electron placed on the 3s orbital of free aluminum leads to a hyperfine constant $A_s^0 = 3\,920$ MHz,[40] the ratio $A_s(Al)/A_s^0$ implies that only a charge of the order $5.10^{-4}e$ has been transferred from the CrO_6^{9-} unit to a close aluminum ion. ENDOR results on $MgAl_2O_4:Cr^{3+}$[41] or $RbCdF_3:Cr^{3+}$[30] also show that the charge of active electrons is essentially confined in the complex formed by the impurity and its six nearest neighbors. The same conclusion has been obtained from ab initio calculations carried out on big clusters.[42]

3. COMPUTATIONAL DETAILS

As pointed out in the introduction, this work is addressed to explore the differences between optical transitions of Cr^{3+} impurities embedded in $LiBaF_3$ and $KMgF_3$ lattices. As active electrons of Cr^{3+} in fluorides have been shown to be essentially localized in the CrF_6^{3-} complex formed by the impurity, and the six nearest neighbors[42,34] calculations have been carried out on CrF_6^{3-} units but subjected to the action of the electrostatic potential from the rest of lattice ions, $\mathbf{V}_R(\mathbf{r})$, generating $\mathbf{E}_R(\mathbf{r})$. This approach has explained the different color of ruby and emerald[19] taking into account that the metal−ligand distance is found to be the same for both systems.[20,21]

The optical transitions have been derived by means of the very accurate wave function-based complete active space self-consistent field method corrected by many-body second-order perturbation theory (CASPT2) first-principles method. This method includes most of the electron correlation energy and usually yields excellent results.[43] We have employed the MOLCAS 6.7 program suite[44] to undertake these calculations. The active space employed was formed by the five mainly 3d(Cr) molecular orbitals, plus the mainly 4s(Cr) one containing a total number of three electrons. In this work, large all-electron atomic natural orbital basis-sets[45] formed by contracting Gaussian functions, so as to reproduce the natural orbitals obtained from correlated calculations on atoms, have been used. In this particular case, we have used 8 contracted gaussians to reproduce the s and p levels of Cr and the s levels of F, 6 gaussians for both the d levels of Cr and the p levels of F, whereas only 2 gaussians for the d levels of F.

As for the potential $\mathbf{V}_R(\mathbf{r})$ in the $LiBaF_3$ and $KMgF_3$ host lattices, it has been simulated by means of a set of point charges (about 250), which are located in lattice positions around the cluster, whose charge value itself is fitted in order to reproduce the potential inside the cluster due to the infinite lattice using an Evjen−Ewald scheme.[46]

As previous calculations of the equilibrium geometry for Cr^{3+}-doped $LiBaF_3$ and $KMgF_3$ within the framework of the DFT show that the $Cr^{3+}-F^-$ distance, **R**, for both systems is the same within 0.7%,[7] we have initially performed calculations on the two systems at **R** = 190 pm. Later on we have looked into the changes of optical transitions due to small variations of the $Cr^{3+}-F^-$ distance. For the sake of completeness, some calculations have also been performed for the isolated CrF_6^{3-} center.

In addition to CASPT2 results, supplementary DFT calculations have also been carried out in order to analyze the subtle changes of covalency in the studied systems. Indeed, in DFT, the electronic density is obtained through only one Slater determinant, which makes easier the analysis of charge distribution. These calculations were performed using the Amsterdam density functional (ADF) program suite.[47] The exchange-correlation functional was computed as proposed by the Vosko−Wilk−Nusair functional[48] in the local density approximation (LDA) and Becke−Perdew (BP86)[49,50] functional in the generalized gradient approximation (GGA). We have verified that the results obtained with all of them provide with very similar results. In this particular case, high quality Slater basis-sets, as provided by the program database and formed by three Slater functions plus a polarization one, were employed.

Table 1.[a]

	$KMgF_3:Cr^{3+}$	$LiBaF_3:Cr^{3+}$
$E(^2E)$	15100	
	17799	17703
$E(^4T_2)$	15150	16720
	13870	16008
$E(^4T_1)$	21930	23809
	21087	23721
$\Delta(^4T_1; ^4T_2)$	6780	7189
	7217	7713

[a] First row: experimental values of optical transitions for $KMgF_3:Cr^{3+}$[5] and $LiBaF_3:Cr^{3+}$.[6] Second row: calculated values by means of the CASPT2 method at **R** = 190 pm. The values of $E(^2E)$, $E(^4T_2)$, $E(^4T_1)$, and $\Delta(^4T_1; ^4T_2) \equiv E(^4T_1) - E(^4T_2)$ are all given in cm^{-1} units.

4. RESULTS AND DISCUSSION

4.1. Excitation Energies at R = 190 pm. The $E(^4T_j)$ $(j = 1, 2)$ and $E(^2E)$ excitation energies obtained by means of CASPT2 calculations for both $LiBaF_3:Cr^{3+}$ and $KMgF_3:Cr^{3+}$ systems at a distance **R** = 190 pm are reported in Table 1 where the corresponding experimental values are also included. Despite the calculations performed at the same R value, the energies, $E(^4T_j)$, of the two $^4A_2 \rightarrow {}^4T_j$ $(j = 1, 2)$ transitions are found to be clearly higher for $LiBaF_3:Cr^{3+}$ than for $KMgF_3:Cr^{3+}$. For instance, a value $E(^4T_2) = 13\,870$ cm^{-1} is found for $KMgF_3:Cr^{3+}$, while in the case of $LiBaF_3:Cr^{3+}$, the calculated value is $E(^4T_2) = 16\,008$ cm^{-1}. This fact thus concurs with previous findings showing that $\mathbf{E}_R(\mathbf{r})$

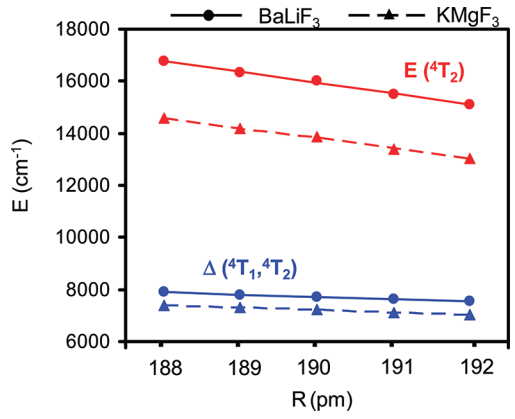

Figure 2. Values of $E(^4T_2)$ and $\Delta(^4T_1; ^4T_2)$ calculated by means of the CASPT2 method for CrF_6^{3-} units embedded in $KMgF_3$ and $LiBaF_3$ lattices as a function of the $Cr^{3+}-F^-$ distance (in pm). All excitation energies are given in cm^{-1}.

in the inverted perovskite enhances the value of $E(^4T_2)$ with respect to what is found in the normal perovskite lattice.[15,16,18] The increase of $E(^4T_j)$ $(j = 1, 2)$ on passing from $KMgF_3:Cr^{3+}$ to $LiBaF_3:Cr^{3+}$ is consistent with experimental findings[5,6] such as those shown in Table 1. Therefore, according to the discussion carried out in the introduction, the difference of 1 500 cm^{-1} between the experimental $E(^4T_2)$ values of $LiBaF_3:Cr^{3+}$ and $KMgF_3:Cr^{3+}$ cannot be mainly due to the presence of a close vacancy in the first system.

It is worth noting that a situation similar to that collected in Table 1 comes out when comparing the optical properties of $KMgF_3:M^{2+}$ and $LiBaF_3:M^{2+}$ (M = Ni, Co, Mn).[12−14] In all these cases, the experimental[12−14] and theoretical[15,16,18] results are consistent with a 10Dq value which is 10−15% higher for $LiBaF_3:M^{2+}$ than when M^{2+} enters $KMgF_3$ despite that the equilibrium $M^{2+}-F^-$ distance is found to be the same within 1%.

It should be noticed now that according to the present CASPT2 calculations, the quantity $\Delta(^4T_1; ^4T_2)$ is not the same in the two studied systems but increases by 500 cm^{-1} on going from $KMgF_3:Cr^{3+}$ to $LiBaF_3:Cr^{3+}$. This result, derived from the present calculations, is consistent with the values $\Delta(^4T_1; ^4T_2)$ = 6 780 and 7 189 cm^{-1} measured for $KMgF_3:Cr^{3+}$ and $LiBaF_3:Cr^{3+}$, respectively.[5,6] Thus, according to these data, the different $\Delta(^4T_1; ^4T_2)$ value displayed by $KMgF_3:Cr^{3+}$ and $LiBaF_3:Cr^3$ can be reproduced merely through the inclusion of the corresponding internal field, $\mathbf{E}_R(\mathbf{r})$, acting on the active electrons confined in the CrF_6^{3-} unit.

In regard to the calculated $E(^2E)$ value, it is found to be nearly independent of $\mathbf{E}_R(\mathbf{r})$, being the same for both $LiBaF_3:Cr^{3+}$ and $KMgF_3:Cr^{3+}$ within 0.5%. As shown in Table 1, the present calculations overestimate a little the position of the ^2E_g state, which is independent of 10Dq.[34]

In the case of Cr^{3+}-doped fluorides, it has been possible to measure the energy of the sharp emission line $^2E(t_{2g}^3) \rightarrow {}^4A_2(t_{2g}^3)$ but only under an applied pressure.[26−28] Indeed, pressure increases the separation between $^4T_2(t_{2g}^2e_g^1)$ and $^2E(t_{2g}^3)$, thus favoring the emission from the last state. The microscopic origin of this fact has recently been discussed.[51] A value $E(^2E)$ = 15 150 cm^{-1} has been measured on $KMgF_3:Cr^{3+}$ under pressure,[5] which is thus practically coincident with $E(^2E)$ = 15 150 cm^{-1} reported for $K_2NaGaF_6:Cr^{3+}$ and $LiCaAlF_6:Cr^{3+}$.[27,28] Thus, although $E(^2E)$ has not been measured for $LiBaF_3:Cr^{3+}$, these values support that $E(^2E)$ for CrF_6^{3-} is nearly insensitive to the electric field, $\mathbf{E}_R(\mathbf{r})$, coming from the lattice ions where the complex is located. Supporting this view, the value $E(^2E)$ = 17 825 cm^{-1} calculated for the isolated CrF_6^{3-} unit differs only by 0.14% from the figure derived for $KMgF_3:Cr^{3+}$ (Table 1).

It is worth noting now that the pattern found for Cr^{3+}-doped fluorides looks very similar to that encountered for Cr^{3+}-doped oxides. For instance, for emerald where $E(^4T_2)$ = 16 180 cm^{-1},[10] $E(^2E)$ is measured to be equal to 14 690 cm^{-1},[23,24] while for $Mg_2AlO_4:Cr^{3+}$, $E(^2E)$ is only 0.27% lower despite $E(^4T_2)$ = 18 520 cm^{-1}.[52]

4.2. Dependence of $E(^4T_2)$, $E(^4T_1)$ and $E(^2E)$ Excitations on the Metal−Ligand Distance. Let us now focus on changes of $E(^4T_j)$ $(j = 1, 2)$ and $E(^2E)$ energies when the $Cr^{3+}-F^-$ distance is varied. The dependence of calculated $E(^4T_2)$ and $\Delta(^4T_1; ^4T_2)$ on **R** is shown in Figure 2 for both $LiBaF_3:Cr^{3+}$ and $KMgF_3:Cr^{3+}$. It can first be noticed that $E(^4T_2)$ strongly depends on **R** by the following:

$$E(^4T_2) = kR^{-n} \quad (1)$$

where the exponent n is found to be equal to 4.96 for $LiBaF_3:Cr^{3+}$ and 5.3 for $KMgF_3:Cr^{3+}$. A very close value (n = 4.90) is obtained making the CASPT2 calculation for an isolated CrF_6^{3-} unit where there is no internal electric field. This fact thus stresses that the strong dependence of $E(^4T_2)$ upon **R** can essentially be understood merely considering the isolated CrF_6^{3-} complex despite the value of k and thus $E(^4T_2)$ do depend on $\mathbf{E}_R(\mathbf{r})$. The microscopic origin of the dependence of $E(^4T_2)$ upon **R** for an isolated CrF_6^{3-} complex has recently been discussed.[51]

Figure 2 reveals that when **R** is reduced, $E(^4T_1)$ increases, but $\Delta(^4T_1; ^4T_2)$ does not remain constant as it also increases progressively. More precisely, from the data collected for Figure 2, it is found that $\partial\Delta(^4T_1; ^4T_2)/\partial\mathbf{R} = -90$ cm^{-1}/pm for both systems. A similar value is obtained when calculations are performed on the isolated CrF_6^{3-} complex, thus pointing out that $\mathbf{E}_R(\mathbf{r})$ plays a secondary role in regard to $\partial\Delta(^4T_1; ^4T_2)/\partial R$.

Variations of the $Cr^{3+}-F^-$ distance lead to values of $\partial E(^2E)/\partial\mathbf{R}$ that are positive but at the same time much smaller than $|\partial\Delta(^4T_1; ^4T_2)/\partial\mathbf{R}|$. More precisely, $\partial E(^2E)/\partial\mathbf{R}$ is found to be around 15 cm^{-1}/pm for the isolated CrF_6^{3-} complex as well as for Cr^{3+}-doped $LiBaF_3$ and $KMgF_3$. Although $dE(^2E)/d\mathbf{R}$ has not been measured for $LiBaF_3:Cr^{3+}$ and $KMgF_3:Cr^{3+}$, a value of $dE(^2E)/d\mathbf{R} \cong 13$ cm^{-1}/pm has been derived from optical measurement under pressure for $LiCaAlF_6:Cr^{3+}$.[28] In the case of ruby, the experimental value $\partial E(^2E)/\partial P = -7$ cm^{-1}/GPa leads to $\partial E(^2E)/\partial\mathbf{R}$ = 27 cm^{-1}/pm,[22,53] a figure that is not only positive but again of the same order as that obtained for CrF_6^{3-} either isolated or embedded in $LiBaF_3$ or $KMgF_3$ lattices.

4.3. Analysis of Multiplets of Transition-Metal Impurities in Insulators. According to the present analysis, the CASPT2 results are able to reproduce (i) the different $\Delta(^4T_1; ^4T_2)$ value measured for $LiBaF_3:Cr^{3+}$ and $KMgF_3:Cr^{3+}$; (ii) the near independence of $E(^2E)$ on the host lattice observed in Cr^{3+}-doped fluorides and oxides; and (iii) the sign and main trends of $\partial E(^2E)/\partial P$ displayed by available data of Cr^{3+} impurities in oxides and fluorides. However, as it was pointed out in the introduction, the usual model giving $E(^2E) = 22.5B$ and $\Delta(^4T_1; ^4T_2) \cong 12B$ is unable to explain why $\partial\Delta(^4T_1; ^4T_2)/\partial\mathbf{R} < 0$, while $\partial E(^2E)/\partial\mathbf{R} > 0$, and at the same time why $|\partial\Delta(^4T_1; ^4T_2)/\partial\mathbf{R}| \gg \partial E(^2E)/\partial\mathbf{R}$.

Seeking to shed light on this puzzling situation, it is now crucial to examine the basis of the model describing the multiplets of

transition-metal complexes only through 10Dq and the Racah parameters. It should be noted that this model, though widely used, is not exact, as it involves several approximations. Indeed, in the traditional quantum mechanical approach, once the Hartree–Fock orbitals are obtained, it is compulsory to take into account the interaction among all possible Slater determinants of the same symmetry for properly calculating the energy of a given state. This way is followed in the CASPT2 calculations. Nevertheless, due to the difficulty of carrying out this configuration interaction (CI) process, the multiplets of transition-metal complexes are approximately treated considering only the CI process restricted to all $t_{2g}^{p}e_{g}^{q}$ configurations, where $p + q = N$, and N means the number of active electrons coming from the central cation.[1,54] This approximation is thus fully similar to the Slater procedure for describing the multiplets of free atoms and ions.[54] For instance, under this approximation the multiplets of the free Cr^{3+} ion are described considering only the 120 determinants associated with the $3d^3$ configuration thus excluding the admixture with configurations like $3d^24s$ or $3d^24p$. Nevertheless, by virtue of the spherical symmetry displayed by a free ion, there are only two, among all $\langle d_i(1)d_j(1)|e^2/r_{12}|d_k(2)d_l(2)\rangle$ matrix elements, which are independent for determining the relative energies of states of a $3d^N$ configuration. Here d_i just means 3d wave functions of free ion. This situation is however not so simple for an octahedral transition-metal complex coming from a $3d^N$ impurity. In these cases, as a result of the symmetry lowering, the number of independent matrix elements increases up to 10[1,54] if we work within the $t_{2g}^{p}e_{g}^{q}$ configurations ($p + q = N$). Moreover, the active electrons are no longer placed in pure d-levels but in t_{2g} and e_g antibonding molecular orbitals, whose energy difference is 10Dq, and are shortly described by

$$|\phi_{j;\mu}\rangle = \alpha_j|d_{j;\mu}\rangle - \beta_j|\chi_{j;\mu}\rangle$$
$$(j = e,t;\mu = 3z^2 - r^2, x^2 - y^2; xy, xz, yz) \quad (2)$$

Here, $|\chi_{j;\mu}\rangle$ just means a linear combination of the valence orbitals of ligands transforming like $|d_{j;\mu}\rangle$.

In this framework, the energies of multiplets are then described in terms of 10Dq and the Coulomb, J, and exchange, K, integrals like $J(yz, xz)$, $J(yz, x^2 - y^2)$, $K(yz, xz)$, or $K(yz, 3z^2 - r^2)$.[1] More precisely, the expressions of $E(^4T_2)$, $E(^4T_1)$, and $E(^2E)$ in terms of these parameters in the strong field approximation[1,54] are

$$E(^4T_2) = 10Dq + 2\{J(yz, x^2 - y^2) - J(yz, xz)\} - 2\{K(yz, x^2 - y^2) - K(yz, xz)\} \quad (3)$$

$$E(^4T_1) = 10Dq + 2\{J(yz, 3z^2 - r^2) - J(yz, xz)\} - 2\{K(yz, 3z^2 - r^2) - K(yz, xz)\} \quad (4)$$

$$E(^2E) = 3K(yz, xz) \quad (5)$$

It can be noted that in this scheme the three excitation energies depend on 10Dq and Coulomb and exchange integrals. For obtaining the expressions used in the building of the Tanabe–Sugano diagrams, it is however necessary to make two additional assumptions:

$$\alpha_e = \alpha_t = \alpha \quad (6)$$

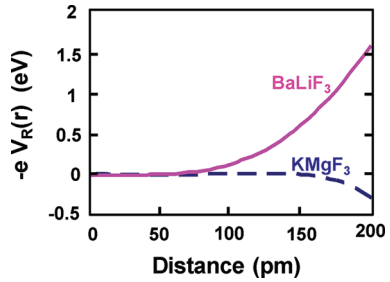

Figure 3. Electrostatic potentials $\mathbf{V}_R(\mathbf{r})$ along a $\langle 100\rangle$ direction on the CrF_6^{3-} complex embedded in $KMgF_3$ and $BaLiF_3$ host lattices displaying normal and inverted perovskite structures, respectively. $\mathbf{V}_R(\mathbf{r})$ comes from all ions of the host lattice lying outside the CrF_6^{3-} unit.

$$\langle\phi_{i;\mu}(1)\phi_{j;\nu}(1)|e^2/r_{12}|\phi_{k;\kappa}(2)\phi_{l;\lambda}(2)\rangle = \alpha^4\langle d_{i;\mu}(1)d_{j;\nu}(1)|e^2/r_{12}|d_{k;\kappa}(2)d_{l;\lambda}(2)\rangle \quad (7)$$

through which spherical symmetry is recovered. This means, for instance, that under these assumptions, $K(yz, x^2 - y^2)$ is strictly equal to $K(yz, xz) = 3B + C$ where

$$B = \alpha^4 B_0 \quad C = \alpha^4 C_0 \quad (8)$$

Here, B_0 and C_0 are the Racah parameters of the free ion provided that the $|d_{j;\mu}\rangle$ wave functions are the same on passing from the free ion to the complex.

In a relevant paper by Florez et al.,[55] all Coulomb and exchange integrals like $J(yz,xz)$, $J(yz,x^2 - y^2)$, $K(yz,xz)$ or $K(yz,3z^2 - r^2)$ were calculated for the MnF_6^{4-} complex. From the results obtained for that system, it turns out that $E(^4T_2)$ in eq 3 would not be exactly equal to 10Dq. The correction given by the quantity $2\{J(yz, x^2 - y^2) - J(yz, xz)\} - 2\{K(yz, x^2 - y^2) - K(yz, xz)\}$ was found to be ~10% of the 10Dq value, thus implying that assumptions depicted in eqs 6 and 7 are not rigorously valid. This fact stresses that $J(yz, x^2 - y^2) \neq J(yz, xz)$ because under O_h symmetry the $|\phi_{e;x^2-y^2}\rangle$ orbital involving σ bonding is not strictly equivalent to the π $|\phi_{t;xy}\rangle$ orbital. Bearing these considerations and eqs 3–5 in mind, it is now possible to qualitatively understand that $\Delta(^4T_1; {}^4T_2)$ and $E(^2E)$ evolve in a different way when pressure is applied or the host lattice is modified. Indeed, when only the CI process is restricted to the $t_{2g}^{p}e_{g}^{q}$ configurations ($p + q = N$), $E(^2E)$ depends on $K(yz, xz)$ involving two orbitals with π bonding. By contrast,

$$\Delta(^4T_1;{}^4T_2) = 2\{J(yz, 3z^2 - r^2) - J(yz, x^2 - y^2)\} - 2\{K(yz, 3z^2 - r^2) - K(yz, x^2 - y^2)\} \quad (9)$$

depends on Coulomb and exchange integrals involving one electron with π bonding but another one with σ bonding.

4.4. Comparison of $LiBaF_3$:Cr^{3+} and $KMgF_3$:Cr^{3+}: Changes of Covalency. From the previous analysis the changes of $\Delta(^4T_1; {}^4T_2)$ on passing from $KMgF_3$:Cr^{3+} to $LiBaF_3$:Cr^{3+} would be the result of a different electric field, $\mathbf{E}_R(\mathbf{r}) = -\nabla\mathbf{V}_R(\mathbf{r})$, undergone by the CrF_6^{3-} complex, which modifies the value of quantities like $J(yz, 3z^2 - r^2)$ or $J(yz, x^2 - y^2)$ and not only 10Dq. The form of the $\mathbf{V}_R(\mathbf{r})$ potential for both $KMgF_3$ and $LiBaF_3$ lattices[16,18] when $\mathbf{r}$ is along a $\langle 100\rangle$ direction is displayed in Figure 3. The $\mathbf{r} = 0$ point denotes the position of the cation to be replaced by the Cr^{3+} impurity. It can be noticed that, in the case of the perovskite lattice, $(-e)\mathbf{V}_R(\mathbf{r})$ is practically flat such as it was early pointed out by Sugano and Shulman[56] and corroborated by subsequent

Table 2. Variation of α_e^2 and α_t^2 Coefficients with the $Cr^{3+}-F^-$ Distance, R, Calculated for $KMgF_3:Cr^{3+}$ (First Row) and $LiBaF_3:Cr^{3+}$ (Second Row)[a]

R	α_e^2	α_t^2
196	0.806	0.861
	0.784	0.858
190	0.800	0.858
	0.782	0.855
184	0.795	0.854
	0.780	0.851

[a] On passing from $KMgF_3:Cr^{3+}$ to $LiBaF_3:Cr^{3+}$, keeping the same **R** value, bigger changes are found for e_g orbitals displaying σ bonding than for π t_{2g} orbitals. The α_e^2 and α_t^2 values given in this table come from a DFT calculation. **R** is given in pm.

works.[57,11] This situation, which is rather similar to that found in elpasolite lattices like K_2NaCrF_6,[58,59] implies that optical properties of CrF_6^{3-} units embedded in this kind of lattice are nearly unaffected by $\mathbf{V}_R(\mathbf{r})$. In contrast, a quite different situation holds in the case of the inverted perovskite $LiBaF_3$ where, such as it is shown in Figure 3, $(-e)\mathbf{V}_R(\mathbf{r})$ increases with $|\mathbf{r}|$ when $|\mathbf{r}| \geq 50$ pm. The origin of this remarkable difference between the shape of $\mathbf{V}_R(\mathbf{r})$ in $KMgF_3$ and $LiBaF_3$ has been discussed in detail.[16,18]

Let us designate by $\mathbf{R}_i$ the position of the i-ligand nucleus of the isolated CrF_6^{3-} unit where a chromium nucleus is at the center. The electrostatic potential seen by an electron of the CrF_6^{3-} complex due to the interaction with all nuclei is usually called the external potential, $v^0_{ext}(\mathbf{r}, \{\mathbf{R}_i\})$.[60] When the complex is not isolated but embedded in a lattice, the new external potential, $v_{ext}(\mathbf{r}, \{\mathbf{R}_i\})$, is simply given by

$$v_{ext}(\mathbf{r}, \{\mathbf{R}_i\}) = v^0_{ext}(\mathbf{r}, \{\mathbf{R}_i\}) + \mathbf{V}_R(\mathbf{r}) \quad (10)$$

By virtue of the Hohenberg−Kohn theorem,[60] the addition of $\mathbf{V}_R(\mathbf{r})$ implies that the ground state electronic density has to be modified unless $\mathbf{V}_R(\mathbf{r})$ is a constant on the complex. This simple reasoning thus suggests that covalency parameters α_e^2 and α_t^2 are not the same for $KMgF_3:Cr^{3+}$ and $LiBaF_3:Cr^{3+}$. Values for α_e^2 and α_t^2 calculated for both systems at **R** = 190 pm are gathered in Table 2 where as expected $\alpha_t^2 > \alpha_e^2$. Moreover, upon passing from $KMgF_3:Cr^{3+}$ to $LiBaF_3:Cr^{3+}$, α_e^2 is found to decrease by 2%, while the reduction undergone by α_t^2 (0.3%) is certainly much smaller. This fact strongly suggests that the covalency in π t_{2g} orbitals is much less influenced by $\mathbf{E}_R(\mathbf{r})$ than that of the more extended e_g orbitals displaying σ bonding. Accordingly, the change of $\mathbf{E}_R(\mathbf{r})$ is expected to produce minor changes on $K(yz, xz)$ and thus $E(^2E)$ but bigger variations on quantities like $J(yz,3z^2 - r^2)$ and $\Delta(^4T_1; {}^4T_2)$. This reasoning explains, albeit qualitatively, the results collected in Table 1.

It should be noticed now that the increase of $\Delta(^4T_1; {}^4T_2)$ on passing from $KMgF_3:Cr^{3+}$ to $LiBaF_3:Cr^{3+}$ cannot be understood through simple models that assume

$$\langle \phi_{e;\mu}(1)\phi_{t;\nu}(1)|e^2/r_{12}|\phi_{e;\kappa}(2)\phi_{t;\lambda}(2)\rangle = \alpha_e^2\alpha_t^2\Lambda_0(\mu;\nu) \quad (11)$$

$$\Lambda_0(\mu;\nu) = \langle d_{e;\mu}(1)d_{t;\nu}(1)|e^2/r_{12}|d_{e;\kappa}(2)d_{t;\lambda}(2)\rangle \quad (12)$$

where $\Lambda_0(\mu;\nu)$ corresponds to the free Cr^{3+} ion. Indeed, according to this simple model, one would expect a higher $\Delta(^4T_1; {}^4T_2)$ value for $KMgF_3:Cr^{3+}$ (where $\alpha_e^2\alpha_t^2 = 0.687$) than for $LiBaF_3:Cr^{3+}$ ($\alpha_e^2\alpha_t^2 = 0.669$), while the contrary is observed experimentally[5,6] and well reproduced by the present CASPT2 calculations. This discrepancy thus means that the introduction of $\mathbf{E}_R(\mathbf{r})$ not only changes the covalency coefficients, α_e^2 and α_t^2, but also modifies the shape of $|d_{j;\mu}\rangle$ and $|\chi_{j;\mu}\rangle$ wave functions on passing from the free ion to the complex embedded in a lattice. Moreover, the so-called metal−ligand and ligand−ligand contributions in $\langle \phi_{e;\mu}(1)\phi_{t;\nu}(1)\ |e^2/r_{12}|\phi_{e;\kappa}(2)\phi_{t;\lambda}(2)\rangle$ cannot be neglected as it is often made.[61]

Looking at the form of $(-e)\mathbf{V}_R(\mathbf{r})$ energy in $LiBaF_3$, it can be noticed that the associated electric field, $\mathbf{E}_R(\mathbf{r})$, forces the electronic cloud to move from the ligands to the central cation.[16,18] This process is carried out enhancing the probability of bonding electrons of being on the impurity, while the opposite happens for the antibonding electrons. As there are more bonding than antibonding electrons, this leads to a net flow of electronic charge from the ligands to the central cation. This reasoning thus explains qualitatively why α_e^2 decreases on passing from $KMgF_3:M$ to $LiBaF_3:M$ (M = Cr^{3+}, Mn^{2+}). However, this decrease of α_e^2 does not lead to a decrease of $\Delta(^4T_1; {}^4T_2)$ as expected from simple models. By contrast, the small reduction of α_t^2 on passing from $KMgF_3$ to $LiBaF_3$ is followed by a diminution of $E(^2E)$.

4.5. Comparison of $LiBaF_3:Cr^{3+}$ and $KMgF_3:Cr^{3+}$: Deformation of e_g Orbitals. From the analysis carried out up to now, it comes out that the internal electric field, $\mathbf{E}_R(\mathbf{r})$, modifies not only the covalency coefficients, α_e^2 and, to a minor extent, α_t^2, but also the shape of $|d_{j;\mu}\rangle$ and $|\chi_{j;\mu}\rangle$ wave functions involved in eq 2. Moreover, this deformation appears to be especially important in the case of the more extended e_g orbitals.

An easy way to explore this deformation of $LiBaF_3:Cr^{3+}$ and $KMgF_3:Cr^{3+}$ comes from the analysis of the 2s−2p hybridization in fluorine ligands, which is allowed in e_g but not in π t_{2g} orbitals.[1,11] Accordingly, the ligand $|\chi_{j;\mu}\rangle$ wave function involved in the description of an e_g orbital can shortly be written as

$$|\chi_{e;\mu}\rangle = c_p|\chi_{p;\mu}\rangle + c_s|\chi_{s;\mu}\rangle \quad (13)$$

where $c_p^2 + c_s^2 = 1$, and $|\chi_{p;\mu}\rangle$ and $|\chi_{s;\mu}\rangle$ just mean linear combinations of the 2p and 2s orbitals of ligands transforming like $|d_{e;\mu}\rangle$, respectively. As a salient feature we have verified that the ratio c_s^2/c_p^2 is not kept constant on passing from $KMgF_3:Cr^{3+}$ to $LiBaF_3:Cr^{3+}$, thus implying that the $|\chi_{e;\mu}\rangle$ wave function is not the same for both systems. More precisely, a value of $c_s^2/c_p^2 = 0.29$ is derived from DFT calculations for $KMgF_3:Cr^{3+}$, while a lower value of $c_s^2/c_p^2 = 0.22$ is obtained for $LiBaF_3:Cr^{3+}$. It should be noted here that a similar pattern was obtained comparing experimental and theoretical results on $KMgF_3:Mn^{2+}$ and $LiBaF_3:Mn^{2+}$.[18]

When a 2p orbital is mixed with a 2s orbital of fluorine in an antibonding e_g level, this fact enhances the electronic density behind a ligand nucleus.[51] However, the action of $(-e)\mathbf{V}_R(\mathbf{r})$ on CrF_6^{3-} embedded in $LiBaF_3$ (Figure 3) forces the valence electrons to be confined in a shorter place than in the case of $KMgF_3$. This fact explains qualitatively why c_s^2/c_p^2 is smaller for Cr^{3+} or Mn^{2+} impurities in the inverted perovskite than in the normal one.

We have verified that the deformation induced by $\mathbf{V}_R(\mathbf{r})$ also acts on $|d_{e;\mu}\rangle$. In the calculations, the radial part of $|d_{j;\mu}\rangle$, $\mathcal{R}_j(\mathbf{r})$ ($j = e, t$), is written as

$$\mathcal{R}_j(r) = \sum_{m=3}^{5} c_j^m P_m(\mathbf{r}) \quad (14)$$

Here, $P_m(\mathbf{r})$ is a fixed basis function, while the c_j^m coefficients are variable and determined in the minimization procedure. In essence, $P_3(\mathbf{r})$, $P_4(\mathbf{r})$, and $P_5(\mathbf{r})$ are the radial 3d, 4d, and 5d wave functions for the free Cr^{3+} ion. An analysis of c_e^m coefficients indicates that the $\mathscr{R}_e(\mathbf{r})$ radial function is more confined for $LiBaF_3:Cr^{3+}$ than for $KMgF_3:Cr^{3+}$. This fact thus tends to increase the value of the interelectronic repulsion when the host lattice is an inverted perovskite and for states having one electron in the antibonding e_g orbital. Therefore, the increase of $\Delta(^4T_1; {}^4T_2)$ when $KMgF_3$ is replaced by $LiBaF_3$ as the host lattice can be qualitatively understood through a higher confinement of e_g electrons in the inverted perovskite.

4.6. Changes Produced Modifying the Cr^{3+}−F^- Distance. Values of α_e^2 and α_t^2 quantities calculated as a function of the Cr^{3+}−F^- distance, **R**, for both $KMgF_3:Cr^{3+}$ and $LiBaF_3:Cr^{3+}$ are displayed in Table 2. It can be noticed that α_e^2 and α_t^2 both slowly decrease when **R** does. A similar pattern is encountered in a DFT calculation on the isolated CrF_6^{3-} complex. It is worth noting now that, in the calculations by Brik and Ogasawara on CrX_6^{3-} (X = F, Cl, Br) units,[62] it is found that α_e^2 and α_t^2 increase progressively when **R** does. The same pattern has been derived in a recent work covering all halide CrX_6^{3-} complexes (X = F, Cl, Br, I).[51]

Using DFT, we have also calculated the energy of the $|xy\uparrow\, xz\uparrow\, yz\downarrow|$ determinant as a function of **R**, finding that it depends linearly on the covalency coefficient α_t^2. These results thus support the fact that the calculated value $\partial E(^2E)/\partial \mathbf{R}$ = 15 cm^{-1}/pm mainly reflects the increase of α_t^2 as far as **R** becomes longer. In contrast, the increase of $\Delta(^4T_1; {}^4T_2)$ when **R** is reduced cannot again be understood considering only the changes experienced by α_e^2 and eqs 11 and 12 based on simplifying assumptions. Seeking to clear out this matter, we have looked into changes undergone by both $\mathscr{R}_e(\mathbf{r})$ and $\mathscr{R}_t(\mathbf{r})$ radial functions when the Cr^{3+}−F^- distance is varied. We have verified that the dominant contributions in eq 14 come from the m = 3 and 4 terms involved in eq 14. On passing from **R** = 196 to 184 pm, the ratio c_e^4/c_e^3 is found to decrease by 9%. In contrast to the case of the π t_{2g} orbital $\mathscr{R}_t(\mathbf{r})$ where it is found to be stiffer when **R** is varied. Indeed, c_t^4/c_t^3 decreases only by 2% when **R** is moved in the same interval.

These results thus support, albeit qualitatively, that the increase of $\Delta(^4T_1; {}^4T_2)$ due to a lessening of the **R** distance is related to the contraction undergone by the antibonding e_g orbital, which is certainly bigger than the corresponding of the π t_{2g} orbital.

5. CONCLUSIONS

The present CASPT2 calculations carried out on CrF_6^{3-} units under the influence of the electric field, $\mathbf{E}_R(\mathbf{r})$, coming from the rest of lattice ions, are able to reproduce the main trends observed on passing from $KMgF_3:Cr^{3+}$ to $LiBaF_3:Cr^{3+}$. In particular, such calculations give a $\Delta(^4T_1; {}^4T_2)$ value, which is higher for the latter than for the former system in agreement with experimental findings.[5,6]

At the same time, the energy, $E(^2E)$, of the $^2E(t_{2g}^3)$ state (relative to that of the ground state $^4A_2(t_{2g}^3)$) is found to be practically insensitive to the host lattice, a fact that concurs with available experimental data for Cr^{3+}-doped fluorides and oxides. Along this line, it is stressed that the energy of excitations where the three active electrons still occupy π t_{2g} orbitals are much less influenced by $\mathbf{E}_R(\mathbf{r})$ than in the case of states involving an electron in the σ e_g orbital, which spreads over a bigger area.

According to the present analysis, the small variations induced by a change of the host lattice or a hydrostatic pressure cannot all be explained using simple recipes based on Tanabe−Sugano diagrams and considering only the changes of covalency. For instance, $\Delta(^4T_1; {}^4T_2)$ is found to increase on going from $KMgF_3:Cr^{3+}$ to $LiBaF_3:Cr^{3+}$, despite that α_e^2 is found to be a little smaller for the last system. A similar situation holds when **R** is reduced. According to the present study, these surprising facts reflect the deformation of $|d_{e;\mu}\rangle$ and $|\chi_{e;\mu}\rangle$ wave functions. In contrast, the present results support that the variation of $E(^2E)$ is related to a good extent to that of α_t^2 describing the covalency in the π t_{2g} orbital.

It should be noticed now that, according to eq 5 and the present discussion, the variations of $E(^2E)$ due to $\mathbf{E}_R(\mathbf{r})$ or a hydrostatic pressure do depend on small changes of electronic density in the π t_{2g} orbital. However, it does not mean at all that the one electron energy of that orbital, $\varepsilon(t_{2g})$, is practically unmodified by $\mathbf{V}_R(\mathbf{r})$. Indeed, it produces a first order shift on $\varepsilon(t_{2g})$ given by $\langle\phi_{t;\mu}|\mathbf{V}_R(\mathbf{r})|\phi_{t;\mu}\rangle$, which appears even if the electronic density in the π t_{2g} orbital is kept frozen. Therefore, at variance with what happens for $E(^2E)$ or $\Delta(^4T_1; {}^4T_2)$, changes on 10Dq induced by $\mathbf{V}_R(\mathbf{r})$ are not necessarily related to the associated variations of electronic density.[63]

Despite the fact that there are optical variables like $E(^4T_2)$ or $\Delta(^4T_1; {}^4T_2)$, which do reflect the influence of $\mathbf{E}_R(\mathbf{r})$, the present analysis shows that quantities like the exponent n in eq 1, $\partial\Delta(^4T_1; {}^4T_2)/\partial\mathbf{R}$, $E(^2E)$, or $\partial E(^2E)/\partial\mathbf{R}$ can be reproduced mainly through the isolated CrF_6^{3-} complex.

When crystal field spectra of a transition-metal impurity in halides are fitted by means of 10Dq and the Racah parameters, it is found that B decreases following the decrease in the halide electronegativity.[4,54] According to the present results, this reduction is not necessarily due only to the increase of covalency that takes place upon passing, for instance, from a MF_6 complex to MBr_6 (M = Cr^{3+}, Co^{2+}, Ni^{2+}, Mn^{2}). Indeed, this fact leads to a total charge on the impurity, M, which is smaller for MBr_6 than for MF_6. This means, in turn, that the $|d_{j;\mu}\rangle$ functions of MBr_6 will be expanded[64,55] with respect to those in MF_6 leading to an additional reduction of the interelectronic repulsion for the bromine complex.

Bearing in mind the similarities between fluorides and oxides doped with Cr^{3+} ions, the present results obtained on the model systems $KMgF_3:Cr^{3+}$ and $LiBaF_3:Cr^{3+}$ can shed light on doped oxides like $Al_2O_3:Cr^{3+}$ or $Be_3Si_6Al_2O_{18}:Cr^{3+}$ where the local symmetry is lower than cubic. Although the color exhibited by these gemstones has been shown to reflect the dependence of 10Dq on $\mathbf{E}_R(\mathbf{r})$,[19,63] it is crucial to clarify whether the differences in color are directly related to the corresponding changes in electronic density. Work on this relevant question is now underway.

■ ACKNOWLEDGMENT

The support by the Spanish Ministerio de Ciencia y Tecnología under Project FIS2009-07083 is acknowledged.

■ REFERENCES

(1) Sugano, S.; Tanabe, Y.; Kamimura, H. *Multiplets of Transition-Metal Ions in Crystals*; Academic Press: New York, 1970.

(2) Henderson, B.; Imbush, G. F. *Optical Spectroscopy of Inorganic Solids*; Oxford Science Publications: Oxford, U.K., 1989.

(3) Powell, R. C. *Physics of Solid State Laser Materials*; Springer: New York, 1998.

(4) Jørgensen, C. K. *Modern Aspects of Ligand Field Theory*; North Holland: Amsterdam, 1971.
(5) Mortier, M.; Wang, Q.; Buzaré, J. Y.; Rousseau, M. *Phys. Rev. B* **1997**, *56*, 3022.
(6) Mortier, M.; Gesland, J. Y.; Pirou, B.; Buzaré, J. Y.; Rousseau, M. *Opt. Mater.* **1994**, *4*, 115.
(7) Moreno, M.; García-Lastra, J. M.; Barriuso, M. T.; Aramburu, J. A. *Theor. Chem. Acc.* **2007**, *118*, 665.
(8) Haussühl, S.; Recker, K.; Leckebus, R. *Z. Naturforsch., A: Phys. Sci.* **1972**, *27*, 1022.
(9) Babel, D.; Tressaud, A. In *Inorganic Solid Fluorides*; Hagenmuller, P., Ed.; Academic Press: New York, 1985.
(10) Burns, R. G. *Mineralogical Applications of Crystal Field Theory*; Cambridge University Press: Cambridge, 1993.
(11) Moreno, M.; Barriuso, M. T.; Aramburu, J. A.; Garcia-Fernandez, P.; Garcia-Lastra, J. M. *J. Phys.: Condens. Matter* **2006**, *18*, R315.
(12) Duarte, M.; Martins, E.; Baldochi, S. L.; Morato, S. P.; Vieira, N. D.; Vieira, M. M. F. *Opt. Commun.* **1998**, *151*, 366.
(13) Mortier, M.; Piriou, B.; Buzare, J. Y.; Rousseau, M.; Gesland, J. Y. *Phys. Rev. B* **2003**, *67*, 115126.
(14) Henke, B.; Secu, M.; Rogulis, U.; Schweizer, S.; Spaeth, J. M. *Phys. Status Solidi C* **2005**, *2*, 380.
(15) Trueba, A.; García-Lastra, J. M.; Barriuso, M. T.; Aramburu, J. A.; Moreno, M. *Chem. Phys.* **2009**, *362*, 82.
(16) Garcia-Lastra, J. M.; Buzare, J. Y.; Barriuso, M. T.; Aramburu, J. A.; Moreno, M. *Phys. Rev. B* **2007**, *75*, 155101.
(17) Nishimatsu, T.; Terakubo, N.; Mizuseki, H.; Kawazoe, Y.; Pawlak, D. A.; Shimamura, K.; Ichinose, M.; Fukuda, T. *Jpn. J. Appl. Phys.* **2003**, *42*, 5082.
(18) Trueba, A.; García-Lastra, J. M.; Barriuso, M. T.; Aramburu, J. A.; Moreno, M. *Phys. Rev. B* **2008**, *78*, 075108.
(19) (a) García-Lastra, J. M.; Barriuso, M. T.; Aramburu, J. A.; Moreno, M. *Phys. Rev. B* **2005**, *72*, 113104. (b) *J. Phys. Chem. A* **2008**, *112*, 1045.
(20) Gaudry, E.; Sainctavit, P.; Juillot, F.; Bondioli, F.; Ohresser, P.; Letard, I. *Phys. Chem. Miner.* **2006**, *32*, 710.
(21) Gaudry, E.; Cabaret, D.; Brouder, C.; Letard, I.; Rogalev, A.; Wilhlem, F.; Jaouen, N.; Sainctavit, P. *Phys. Rev. B* **2007**, *76*, 094110.
(22) Jahren, A. H.; Kruger, M. B.; Jeanloz, R. J. *J. Appl. Phys.* **1992**, *71*, 1579.
(23) Wood, D. L. *J. Chem. Phys.* **1965**, *42*, 3404.
(24) Fonger, W. H.; Struck, C. W. *Phys. Rev. B* **1974**, *11*, 3251.
(25) Duclos, S.; Vohra, Y. K.; Ruoff, A. L. *Phys. Rev. B* **1990**, *41*, 5372.
(26) Freire, P. T. C.; Pilla, O.; Lemos, V. *Phys. Rev. B* **1994**, *49*, 9232.
(27) Dolan, J. F.; Rinzler, A. G.; Kappers, L. A.; Bartram, R. H. *J. Phys. Chem. Solids* **1992**, *53*, 905–912.
(28) Sanz-Ortiz, M. N.; Rodriguez, F.; Hernández, I.; Valiente, R.; Kück, S. *Phys. Rev. B* **2010**, *81*, 045114.
(29) Patel, J. L.; Davies, J. J.; Cavenett, B. C.; Takeuchi, H.; Horai, H. *J. Phys. C* **1976**, *9*, 129.
(30) Studzinski, P.; Spaeth, J. M. *Phys. Status Solidi B* **1986**, *136*, 735.
(31) Du Varney, R. C.; Niklas, J. R.; Spaeth, J. M. *Phys. Status Solidi B* **1981**, *103*, 329.
(32) Binois, M.; Leble, A.; Rousseau, J. J.; Fayet, J. C. *J. Phys. Colloq.* **1973**, *C9* (34), 285.
(33) Takeuchi, H.; Arakawa, M.; Aoki, H.; Yosida, T.; Horai, K. *J. Phys. Soc. Jpn.* **1982**, *51*, 3166.
(34) Garcia-Fernandez, P.; Trueba, A.; García-Cueto, B.; Aramburu, J. A.; Barriuso, M. T.; Moreno, M. *Phys. Rev. B* **2011**, *83*, 125123.
(35) Kohn, W. *Many Body Physics*; Gordon and Breach: New York, 1968.
(36) Resta, R. *Eur. Phys. J. B* **2011**, 79,121.
(37) Reinen, D. *Struct. Bonding* **1969**, *6*, 30.
(38) Jeck, R. K.; Krebs, J. J. *Phys. Rev. B* **1972**, *5*, 1677.
(39) Laurance, N.; McIrvine, E. C.; Lambe, J. *J. Phys. Chem. Solids* **1962**, *23*, 515.
(40) Weil, J. A.; Bolton, J. R.; Werz, J. E. *Electron Paramagnetic Resonance*; Wiley: New York, 1964.
(41) Bravo, D.; Bottcher, R. *J. Phys.: Condens. Matter* **1992**, *4*, 7295.
(42) García-Lastra, J. M.; Barriuso, M. T.; Aramburu, J. A.; Moreno, M. *J. Phys.: Condens. Matter* **2010**, *22*, 155502.
(43) Andersson, K.; Malmqvist, P. A.; Roos, B. O. *J. Chem. Phys.* **1992**, *96*, 1218.
(44) Andersson, K.; Aquilante, F.; Barysz, M.; Bednarz, E.; Bernhardsson, A.; Blomberg, M. R. A.; Carissan, Y.; Cooper, D. L.; Cossi, M.; Devarajan, A.; De Vico, L.; Ferré, N.; Fülscher, M. P.; Gaenko, A.; Gagliardi, L.; Ghigo, G.; de Graaf, C.; Hess, B. A.; Hagberg, D.; Holt, A.; Karlström, G.; Krogh, J. W.; Lindh, R.; Malmqvist, P.-Å.; Nakajima, T.; Neogrády, P.; Olsen, J.; Pedersen, T. B.; Raab, J.; Reiher, M.; Roos, B. O.; Ryde, U.; Schimmelpfennig, B.; Schütz, M.; Seijo, L.; Serrano-Andrés, L.; Siegbahn, P. E. M.; Stålring, J.; Thorsteinsson, T.; Veryazov, V.; Widmark, P.-O.; Wolf, A. *MOLCAS 7.0*; Lund University: Sweden, 2007.
(45) Roos, B. O. *New Challenges in Computational Quantum Chemistry*; Broer, R., Aerts, P. J. C., Bagus, P. S., Eds.; Groningen: Netherlands, 1994; p 12.
(46) (a) Piken, A. G.; Van Gool, W. *Ewald Program*; Technical Report SL 68-10 for Ford Motor Co. 1968.
(47) te Velde, G.; Bickelhaupt, F. M.; Baerends, E. J.; Guerra, C. F.; Van Gisbergen, S. J. A.; Snijders, J. G.; Ziegler, T. *J. Comput. Chem.* **2001**, *22*, 931.
(48) Vosko, S. H.; Wild, L.; Nusair, M. *Can. J. Phys.* **1980**, *58*, 1200.
(49) Becke, A. D. *Phys. Rev. A* **1988**, *38*, 3098–3100.
(50) Perdew, J. P. *Phys. Rev. B* **1986**, *33*, 8822–8824.
(51) Trueba, A.; Garcia-Fernandez, P.; Garcia-Lastra, J. M.; Aramburu, J. A.; Barriuso, M. T.; Moreno, M. *J. Phys. Chem A* **2011**, *115*, 1423.
(52) Wood, D. L.; Imbusch, G. F.; Macfarlane, R. M.; Kisliuk, P.; Larkin, D. M. *J. Chem. Phys.* **1968**, *48*, 5255.
(53) Syassen, K. *High Press. Res.* **2008**, *28*, 75.
(54) Griffith, J. S. *The Theory of Transition Metal Ions*; Cambridge University Press: Cambridge, U.K., 1961.
(55) Florez, M.; Seijo, L.; Pueyo, L. *Phys. Rev. B* **1986**, *34*, 1200.
(56) Sugano, S.; Shulman, R. G. *Phys. Rev.* **1963**, *130*, 517.
(57) Emery, J.; Leble, A.; Fayet, J. C. *J. Phys. Chem. Solids* **1981**, *42*, 789.
(58) Barandiarán, Z.; Pueyo, L. *J. Chem. Phys.* **1983**, *79*, 1926.
(59) Pierloot, K.; Van Praet, E.; Vanquickenborne, L. G. *J. Chem. Phys.* **1992**, *96*, 41.
(60) Parr, R. G.; Yang, W. *Density-Functional Theory of Atoms and Molecules*; Oxford University Press: New York, 1989.
(61) Curie, D.; Barthou, C.; Canny, B. J. *Chem. Phys.* **1974**, *61*, 3048.
(62) Brik, M. G.; Ogasawara, K. *Phys. Rev. B* **2006**, *74*, 045105.
(63) Garcia-Lastra, J. M.; Barriuso, M. T.; Aramburu, J. A.; Moreno, M. *Phys. Rev. B* **2008**, *78*, 085117.
(64) Marshall, W.; Stuart, R. *Phys. Rev.* **1961**, *123*, 2048.